Translational Oncology
www.transonc.com

Volume 12 Number 1 January 2019 pp. 180–189 180

Subcutaneous Inoculation of 3D Pancreatic Cancer Spheroids Results in Development of Reproducible Stroma-Rich Tumors

Mikhail Durymanov[*], Christian Kroll[*], Anastasia Permyakova[*], Elizabeth O'Neill[†], Raed Sulaiman[‡], Michael Person[§] and Joshua Reineke[*]

[*]Department of Pharmaceutical Sciences, South Dakota State University, Brookings, SD; [†]Avera Medical Group Oncology and Hematology, Sioux Falls, SD; [‡]Department of Pathology and Laboratory Medicine, Avera McKennan Hospital, Sioux Falls, SD; [§]Surgical Institute of South Dakota, Sioux Falls, SD

Abstract

Pancreatic ductal adenocarcinoma (PDAC) is a deadly disease characterized by high expression of extracellular matrix in tumor tissue, which contributes to chemoresistance and poor prognosis. Here, we developed 3D pancreatic cancer spheroids, based on pancreatic cancer cells and fibroblast co-culture, which demonstrate innate desmoplastic properties and stay poorly permeable for model nanoparticles. Our study revealed that establishment of tumors by transplantation of spheroids significantly improved subcutaneous xenograft model of PDAC, which stays the most widely used animal model for testing of new drugs and drug delivery approaches. Spheroid based tumors abundantly produced different extracellular matrix (ECM) components including collagen I, fibronectin, laminin and hyaluronic acid. These tumors were highly reproducible with excellent uniformity in terms of ECM architecture recapitulating clinical PDAC tumors, whereas in more common cell based xenografts a significant intertumor heterogeneity in extracellular matrix production was found. Moreover, spheroid based xenografts demonstrated higher expression of pro-fibrotic and pro-survival PDAC hallmarks in opposite to cell based counterparts. We believe that future development of this model will provide an effective instrument for testing of anti-cancer drugs with improved predictive value.

Translational Oncology (2019) 12, 180–189

Introduction

High expression of extracellular matrix (ECM) components in tumors remains a significant challenge for effective drug delivery and therapy of some forms of cancer including pancreatic ductile adenocarcinoma (PDAC) [1,2]. In the case of PDAC, the desmoplastic reaction develops in tumor tissue resulting in deposition of such ECM components as collagens I and III, fibronectin, laminin, hyaluronic acid and others [1]. The main source of ECM are cancer associated fibroblasts (CAFs), which originate from pancreatic stellate cells (PSCs) and resident fibroblasts upon activation induced by factors secreted by cancer cells [3–6]. Obviously, ECM is an important participant in a cross-talk between cancer and stromal cells, but its contribution to PDAC progression at different stages is not fully understood. It seems that ECM remodeling, including bundling and cross-linking in advanced PDAC, plays an active role in pro-metastatic potential and drug resistance [7]. In particular, collagen I induces epithelial-mesenchymal transition (EMT) and mediates both invasion and chemoresistance [8–10]. Laminin as well as fibronectin also contribute to cell proliferation, survival and metastases [11,12]. Hyaluronan is involved in increased cancer cell proliferation and migration [13]. Additionally, this glycosaminoglycan significantly contributes to elevated stromal fluid pressure, impeding diffusion of

Address all correspondence to: Dr. Joshua Reineke, Assistant Professor, Department of Pharmaceutical Sciences, College of Pharmacy, South Dakota State University, 1055 Campanile Avenue, SAV 257, Avera Health Science Building, Box 2202C, Brookings, SD, 57007, USA. E-mail: joshua.reineke@sdstate.edu
Received 21 August 2018; Revised 2 October 2018; Accepted 2 October 2018

1936-5233/19
https://doi.org/10.1016/j.tranon.2018.10.003

anti-cancer drugs in the tumor interstitium and causing collapse of lymphatic and blood vessels that results in impaired diffusion and therapeutic molecule uptake [14,15].

Here, we developed a 3D spheroid model resembling avascular microtumors, able to innate production of complex fibrillar ECM. Some attempts for development of pancreatic cancer spheroids were made earlier [16,17], but for obtained microtumors the impact of stromal cells on ECM production, composition and organization was not determined. Moreover, we translated our spheroid model *in vivo* and compared it with clinical tumors aiming at providing an alternative to costly genetically engineered mouse models and improving conventional subcutaneous xenograft PDAC models, which is the most widely used model in pre-clinical translational studies so far.

Materials and Methods

Cell Culture

Human pancreatic ductal adenocarcinoma PANC-1 (ATCC CRL-1469) cell line and embryonic mouse fibroblasts NIH3T3/GFP (Cell Bioalbs, Inc.) permanently expressing green fluorescent protein, hereafter referred as 3 T3, were cultured in DMEM growth medium supplemented with 10% fetal bovine serum. All cultured cells were grown at 37 °C in a humidified 5% CO_2 atmosphere. Passages 3–15 were used in this study for both cell lines.

Generation of 3D Pancreatic Microtumors

For generation of 3D spheroids, PANC-1 or PANC-1 and 3 T3 cells were seeded onto round-bottomed 96-well plate with ultra-low attachment coating (Corning, Kennebunk, ME) at various ratios in a volume of 100 μL. After 3, 7 or 14 days of incubation at 37 °C in humidified 5% CO_2 atmosphere, spheroids were processed for other experiments. For two-week-old microtumors, additional 100 μL of growth medium were added to each well upon 1 week incubation. For some experiments, spheroids were grown in a medium containing bFGF, or anti-β1-integrin IgG at concentrations of 10 ng mL^{-1} and 18 μg mL^{-1}, respectively.

Measurement of Spheroid Diameters and Cell Viability

Spheroid images in transmitted light were obtained using an inverted Axio Observer A1 microscope (Carl Zeiss, G ttingen, Germany) equipped with ×20/0.4 objective lens. Spheroid diameters were measured using the instrument software.

Cell viability in spheroids was measured by caspase activity assay using Caspase-Glo 9 kit (Promega, Madison, WI) according to manufacturer's manual with minor changes. Each sample contained 10–12 spheroids in PBS collected in one well of a 96-well plate. As a negative control (maximal cell viability), 2D cultured PANC-1 cells with confluency of 70% were used. The positive control (maximal caspase activity) was a sample with 3D PANC-1 spheroids after 48 h incubation with 20 μM of doxorubicin. Obtained values of luminescence, measured using 96-well plate spectrophotometer SpectraMax M2 (Molecular Devices, Sunnyvale, CA), were normalized by protein content, determined by Bradford assay.

Nanoparticle Penetration to Microtumors

Fluorescent latex FluoSpheres beads (Molecular Probes, Eugene, OR) with mean diameters of 20 nm (F8786), 100 nm (F8801), and 500 nm (F8812) were chosen as model particles for penetration analysis. Their physicochemical characteristics such as size and ζ-potential were measured by DLS using Zetasizer Nano ZS (Malvern Instruments Ltd., Malvern, UK). Nanoparticles were added to two-week-old PANC-1 or PANC-1/3 T3 (grown at initial cell number of 120 or 120:12, respectively) spheroids at final concentrations of 20 μg mL^{-1} and incubated for 24 hours. Spheroids were then washed twice with PBS to remove non-bound nanoparticles, frozen in HistoPrep tissue embedding medium, and cut into 10 μm sections using the Leica CM1510 cryotome (Leica, Wetzlar, Germany). To stain the cell nuclei, spheroid sections were incubated in 1 μg mL^{-1} Hoechst 33342 (Tocris Bioscience, Bristol, UK) in water for 5 minutes and air-dried before imaging.

Animal Xenograft Model and Clinical PDAC Tumors

Tumor cell based xenografts were established by subcutaneous injection of 3×10^6 PANC-1 cells or 3×10^6 PANC-1 and 3×10^5 3 T3 cells into the right flank of athymic NU/J (homozygous Foxn1 < nu>) 7-week-old male mice (Jackson Laboratory, Ban Harbor, ME). For inoculation of spheroid-based tumors, around 150 two-week-old PANC-1 or PANC-1/3 T3 (grown at initial cell number of 120 or 120:12, respectively) spheroids were implanted subcutaneously into the right flank of mice. Tumors were measured with calipers daily starting at day 7 post inoculation. Tumor volumes were calculated according to the formula $V = (\text{long axis} \times \text{short axis}^2)/2$. All animals were maintained in specific pathogen-free conditions with water and feed *ad libitum*. All animal experiments were approved by the South Dakota State University Institutional Animal Care and Use Committee.

Collection of human tumor tissues was approved by the Internal Review Boards of South Dakota State University and Avera Medical Group. Signed informed consent from patients for research use of pancreatic tumor tissue in this study was obtained prior to acquisition of the specimen. Samples were confirmed to be tumor tissue based on pathological assessment.

Immunostaining of Frozen Spheroid and Tumor Sections

Excised mouse or human tumors, or 3D spheroids, were washed with PBS and embedded in HistoPrep tissue embedding medium, snap-frozen in liquid nitrogen, and kept at −80 °C. Then the frozen tumor blocks were cut into 10 μm sections, fixed in acetone-methanol (1:1) mixture for 15 min, and air-dried at room temperature.

To determine ECM components, cryosections were immunostained with rabbit monoclonal anti-fibronectin primary antibodies (ab2413, Abcam), rabbit polyclonal anti-type I collagen antibodies (ab34710, Abcam), rabbit polyclonal anti-laminin antibodies (ab11575, Abcam), and sheep polyclonal anti-hyaluronic acid antibodies (ab53842, Abcam). Secondary antibodies were goat anti-rabbit IgG labeled with Alexa Fluor 488 (ab150077, Abcam) or donkey anti-sheep conjugated with Alexa Fluor 568 (ab150077, Abcam). Primary and secondary antibodies were applied at dilutions of 1:200 and 1:300, respectively.

Confocal Microscopy and Image Analysis

Images of all spheroid and tumor sections were obtained using Olympus Fluoview FV1200 confocal laser scanning microscope (Olympus Corporation, Tokyo, Japan) equipped with ×20/0.45 objective lens. Positive fluorescent areas of ECM components in spheroid and tumor sections were determined in 5 different spheroids or in 4 random areas of tumor (in 4 tumors per group, except clinical tumors, where two tumors were analyzed).

For quantitative analysis of nanoparticle penetration in spheroids, the images of spheroid sections were processed in ImageJ software (1.42v, US National Institutes of Health, USA).

Western Blotting

Tumor tissues were lysed in 5% Triton X-100 buffer followed by centrifugation (20,000×*g*, 4 °C, 15 minutes) and collecting of supernatants. Equal amounts of protein (10 μg) were mixed with loading dye, boiled for 5 min, separated on a denaturing SDS-polyacrylamide gel and transferred to a PVDF membrane. The membrane was blocked in 5% dry milk or BSA in TBS buffer with 0.1% Tween (TBS-T) for 1 hour and incubated overnight with antibodies against α-smooth muscle actin (ab7817, Abcam), transforming growth factor β (3711, Cell Signaling), β1-integrins (ab183666, Abcam), phosphorylated AKT1 (ab81283, Abcam), or β-actin (4967, Cell Signaling) as a reference. Then, the membrane was washed twice with TBS-T and incubated with HRP-conjugated secondary antibody (ab6721, Abcam or sc-2005, Santa Cruz Biotechnology) at room temperature for 1 h, followed by several washings with TBS-T and deionized water. Protein bands were visualized by ChemiDoc XRS+ imaging system (Bio-Rad Laboratories, Hercules, CA) using chemiluminescence mode.

Results

Influence of Composition and Term of Cultivation on Final Spheroid Size and Cell Viability

For generation of *in vitro* 3D pancreatic tumor spheroids, we used round-bottomed 96-well plates with non-adherent coating. Formation of pancreatic microtumors takes place within 2–3 days resulting in spherical organoids for both PANC-1 and PANC-1/3 T3 spheroids (Figure 1*A*). Next, we determined how 3 T3 fibroblasts are distributed within spheroids. Since fibroblasts were permanently GFP expressing, we used confocal microscopy for this purpose. Intravital imaging of heterospheroids indicated relatively uniform spatial distribution of 3 T3 cells within a spheroid (Figure 1*B*). However, some extent of fibroblast clustering was observed that mimics the regions of PDAC tumor tissue, where clumps of cancer cells are surrounded by PSCs [18].

Increase of initial cell number per well led to formation of spheroids with higher diameters. Interestingly, there is no increase in spheroid size between day 3 and day 7 (Figure 1, *C* and *D*). In some cases, reduction of spheroid diameter was observed during this time period that could be explained by reinforcement of cell–cell interactions resulting in cell compaction. Between day 7 and day 14, when additional volume of growth medium was added, almost 2-fold increase of spheroid diameter was observed (Figure 1, *C* and *D*).

Active cell proliferation in pancreatic microtumors leads to formation of distant to spheroid surface hypoxic regions, where apoptotic processes occur. To determine viability of cells in spheroids depending on their size, term of cultivation, and composition, we measured caspase 9 activity (Figure 1, *E* and *F*). It was found that detectable (relatively minimal) increase of apoptosis takes place starting after 1 week of incubation. As far as no change in spheroid size happens between day 3 and day 7, an observed growth of caspase activity might be due to the mentioned increase of cell compaction and an increased diffusion barrier for oxygen and other nutrients. It should be noted that in tumors the maximal distance between blood vessels usually does not exceed 200 microns that corresponds to oxygen diffusion limit [19]. It turned out that in a spheroid model a drastic increase of caspase activity on day 7 and later happens if the size of microtumors was more than 400 microns. It is important to note that after 2 weeks of cultivation the level of caspase activity in heterospheroids was less than in case of homospheroids. Most probably, this fact reflects the stimulatory pro-survival effect of fibroblasts on PANC-1 cells, reported earlier for PSC and pancreatic cancer cell co-culture [20].

Production of Different ECM Components in 3D Pancreatic Spheroids

As mentioned above, desmoplastic reaction is a major hallmark of PDAC tumors. As reported earlier, such ECM components as collagen I [8–10], fibronectin [12,21], hyaluronic acid [14] and laminin [11,22] play an important role in development of PDAC and are abundantly expressed in clinical tumors. We aimed to test whether pancreatic microtumors are able to produce these components of ECM. However, immunofluorescent staining of spheroid frozen sections indicated a diffused character of collagen I distribution throughout the cytoplasm of PANC-1 cells in homospheroids without formation of a developed fibrotic scaffold (Figure 2*A*). In contrast, in PANC-1/3 T3 spheroids, formation of an extracellular fibrillar collagen I network was clearly detected. Moreover, high amounts of fibronectin was deposited in heterospheroids, whereas its expression in homospheroids was not observed (Figure 2*B*). This indicates that fibronectin production occurs exclusively due to the contribution of fibroblasts either directly or indirectly through signaling. Perhaps, the formation of the fibronectin fibrillary network in only the PANC-1/3 T3 3D *in vitro* model (and not PANC-1 homospheroids) explains why collagen I fibril assembly does not take place in homospheroids of PANC-1. Fibronectin, along with cell-associated β1-integrin receptors, are key organizers of collagen I fibrillogenesis [23]. As a result of the lacking fibronectin production in homospheroids collagen I polymerization is inhibited/prevented. In contrast, fibronectin polymerization in PANC-1/3 T3 spheroids occurs only with assistance of membrane-associated β1-integrin receptors on the surface of fibroblasts and cancer cells. Supporting this hypothesis, we found that cultivation of heterospheroids in the presence of anti-β1-integrin IgG led to significant decrease in the assembly of fibronectin fibrils (Supplementary Fig. 1) indicating the importance of β1-integrins for ECM assembly and organization.

Besides collagen I, laminin and hyaluronic acid were detected in PANC-1 spheroids (Figure 2*C*). In heterospheroids the content of hyaluronic acid was slightly higher, whereas no difference in laminin deposition was observed. Thus, 3D co-culturing of pancreatic tumor cells PANC-1 and 3 T3 fibroblasts better mimics tumor stroma than the PANC-1 homospheroid tumor model.

For additional stimulation of ECM deposition, treatment of spheroids with basic fibroblast growth factor (bFGF) was used. bFGF is a mitogenic pro-survival molecule which contributes to promotion of fibrosis and cancer cell invasion in PDAC [24]. However, we did not find any significant impact of added bFGF on ECM production in pancreatic microtumors. This is likely due to internal bFGF production by PANC-1 cells [24] already stimulating fibrosis within spheroids. External bFGF slightly increased hyaluronic acid content in both PANC-1 and PANC-1/3 T3 spheroids and laminin deposition in homospheroids (Figure 2*D*).

Study of Size-Dependent Barrier Function in Pancreatic Microtumors to Model Nanoparticles

Desmoplastic reaction of tumor stroma in PDAC is considered as a one of the major barriers towards efficient chemotherapy. Viscous extracellular matrix impairs diffusion of both small molecule chemotherapeutics and nanomedicines reducing their penetration

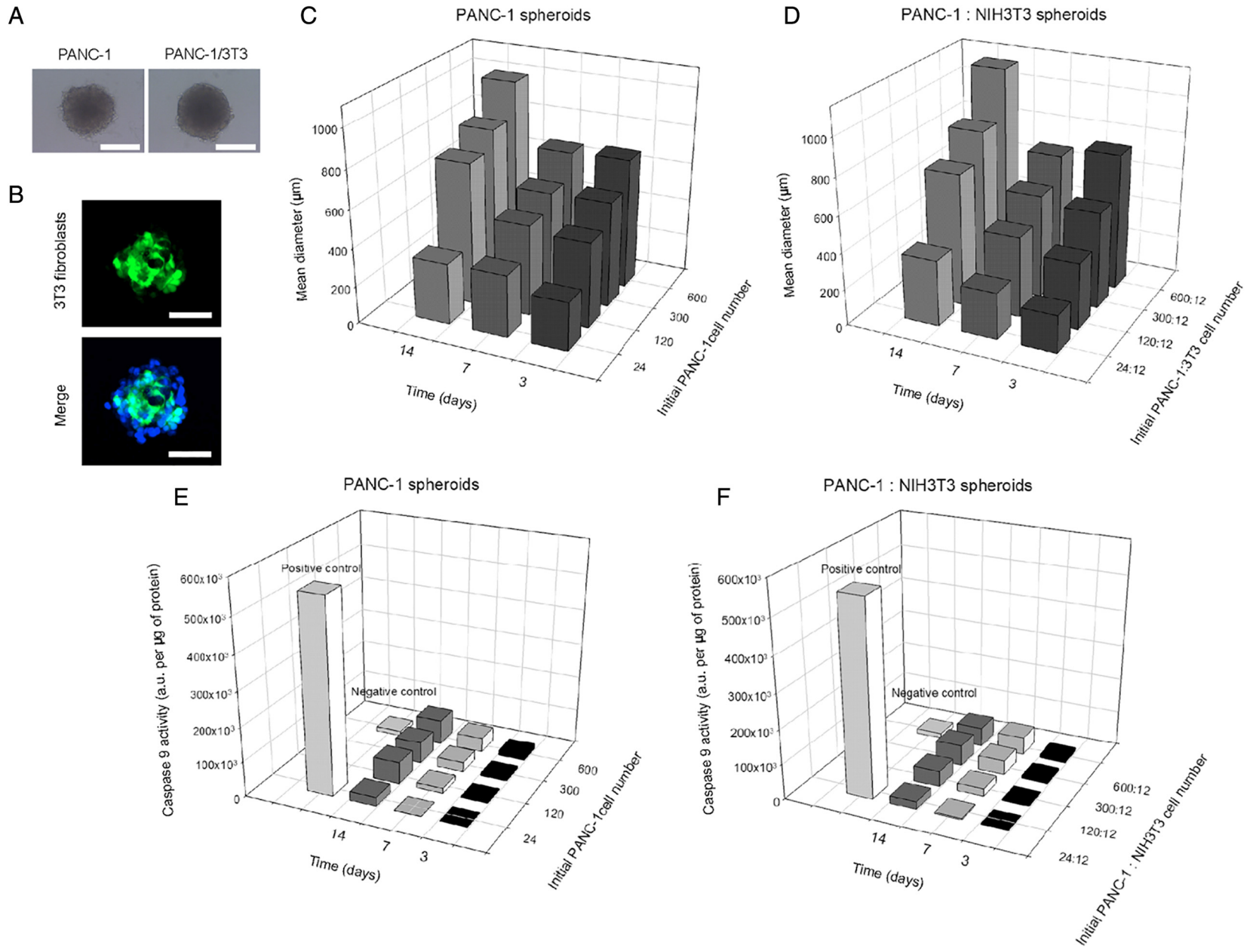

Figure 1. Spheroid formation and growth. (A) Representative images of two-week-old PANC-1 and PANC-1/3 T3 microtumors formed in a round-bottomed well plate at initial cell number of 120 and 120:12 cells, respectively. Scale bar is 500 μm. (B) Distribution of 3 T3 GFP-expressing fibroblasts (green) in 3-day-old heterospheroids formed at initial cell ratio 24:12. Scale bar is 100 μm. (C) and (D) demonstrate dependence of PANC-1 and PANC-1/3 T3 spheroid size on term of incubation and initial cell number. Spheroid diameters were measured microscopically (>10 spheroids for each group). (E) and (F) represent apoptotic activity (estimated by luminescent measurements of caspase-9 activity) in PANC-1 and PANC-1/3 T3 spheroids. Negative control is 2D PANC-1 cells with confluency of 70%. Positive control is 3D spheroids after 48 h incubation with high dose of doxorubicin (20 μM).

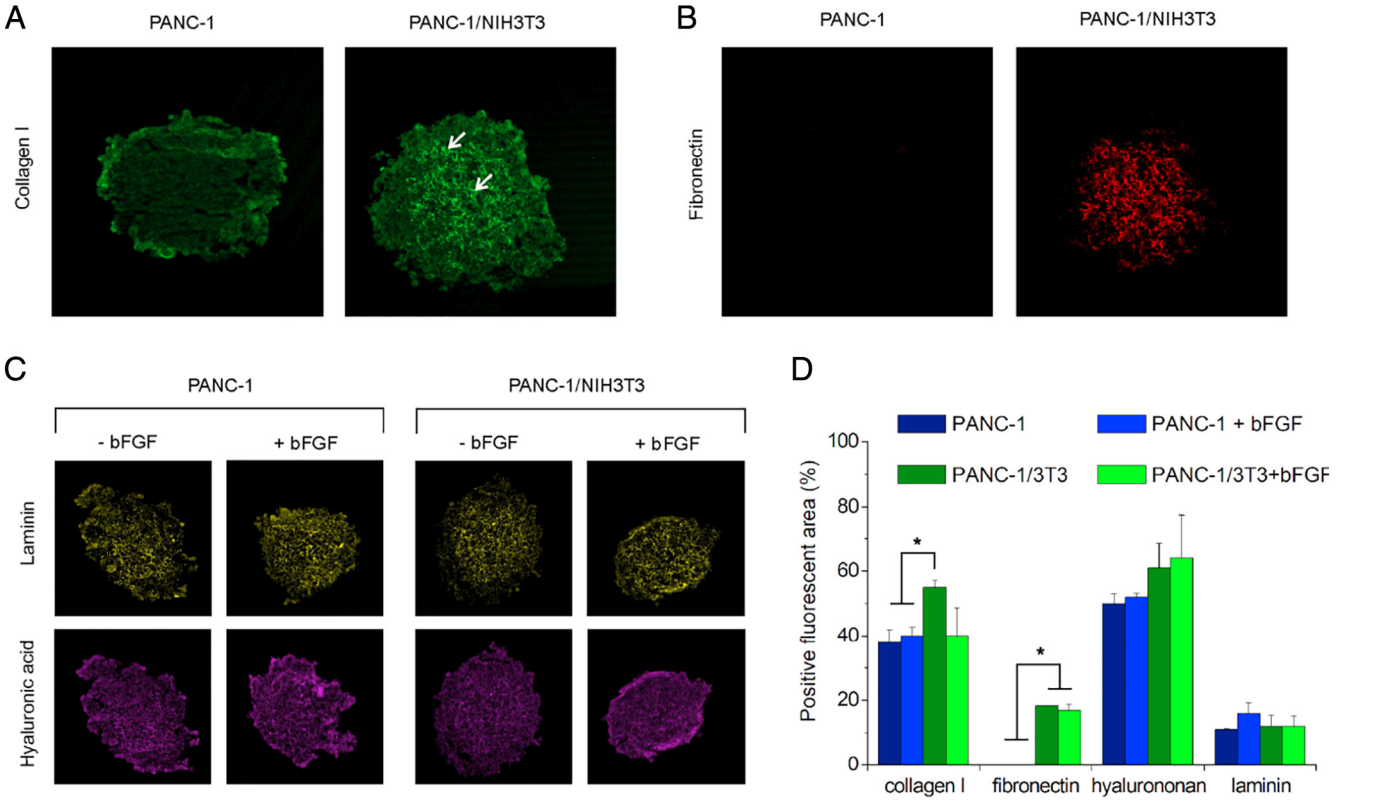

Figure 2. Expression of ECM components in pancreatic cancer spheroids. (A) Visualization of collagen I in PANC-1 and PANC-1/NIH3T3 spheroids. Collagen I was defined in 10 μm-thick spheroid frozen section with anti-collagen I antibodies (green). Collagen I fibrils in heterospheroids are indicated with white arrows. (B) Visualization of fibronectin network (red) in PANC-1/NIH3T3 microtumors and its absence in PANC-1 spheroids. (C) Representative images of spheroid sections stained with antibodies against hyaluronan (purple) and laminin (yellow). Sections were obtained from spheroids incubated for 2 weeks in a presence or absence of 10 ng mL^{-1} human bFGF in growth medium. All spheroid images in (A), (B) and (C) have a size of 635 × 635 microns. (D) Positive fluorescence area of spheroid sections stained with antibodies to different ECM components. For quantification the positive area of binary images in fluorescent channel was normalized on total spheroid area. *$P < .05$ (one-way ANOVA followed by post-hoc Tukey's test). All values are shown as means ± SD.

in tumor tissue [25]. Moreover, ECM overexpression contributes to elevated intratumoral fluid pressure that impedes convective influx of therapeutic molecules/particles to tumor interstitium [25]. Spheroid models ideally mimic the lack of the convective component in penetration of therapeutics. To study the barrier function of the generated pancreatic cancer spheroids for nanoparticles, we used model fluorescent-labeled polystyrene beads of different diameters ranging from 20 nm to 500 nm (Supplementary Table 1). As expected, efficacy of nanoparticle penetration was size-dependent. Smaller nanoparticles better diffused in PANC-1 and PANC-1/3 T3 spheroid stroma, accumulating to a small extent even in a central area (Figure 3, *A-C*). Limited number of 100 nm nanoparticles also reached the central core (Figure 3, *A*, *B* and *D*), whereas 500 nm particles deposited mainly in the outer cell layer primarily due to cellular uptake (Figure 3, *A*, *B* and *E*). Despite larger size, 100 nm particles accumulated to a similar or even better extent in the outer cell layers (up to 70 µm from the surface) of both homo- and heterospheroids, as compared with 20 nm beads. This phenomenon might be attributed to more effective endocytosis of 100 nm microspheres by the cells as compared with 20 nm counterparts.

It should be noted that PANC-1/3 T3 spheroids turned out to be less permeable for nanoparticles of all considered diameters than homospheroids (Figure 3, *A-E*). For example, in homospheroids 10 to 20% of nanoparticles penetrated to a distance further than 35 microns, whereas in heterospheroids this value was less than 10%. As a result, 1.5–2-fold decrease in total nanoparticle uptake by PANC-1/3 T3 spheroids was observed for 20 and 100 nm particles (Figure 3*F*). As mentioned above, heterospheroids express higher amounts of fibrillary collagen I and fibronectin that most likely enhance their ECM viscosity and impair nanoparticle permeability. Thus, heterospheroids better mimic PDAC tumor tissue than homospheroids in terms of permeability for nanoparticles.

Tumorigenicity Comparison of PANC-1 Tumor Xenografts Established by Subcutaneous Injection of Cells Versus Spheroids

It has been shown that generated pancreatic cancer spheroids producing complex fibrous ECM network recapitulate small avascular tumors. We hypothesized that use of spheroids instead of suspension of pancreatic cancer cells for establishing tumors might improve xenograft PDAC mouse models, which relevancy to clinical PDAC tumors is challenged [26,27]. Our hypothesis is based on the important role of hypoxia in PDAC tumor progression. Actually, robust ECM deposition along with expansion of spheroid size promote hypoxic conditions in the spheroid core that can contribute to apoptotic processes indicated in large microtumors (>400 microns in diameter) after long cultivation (Figure 1, *E* and *F*). Hypoxia is

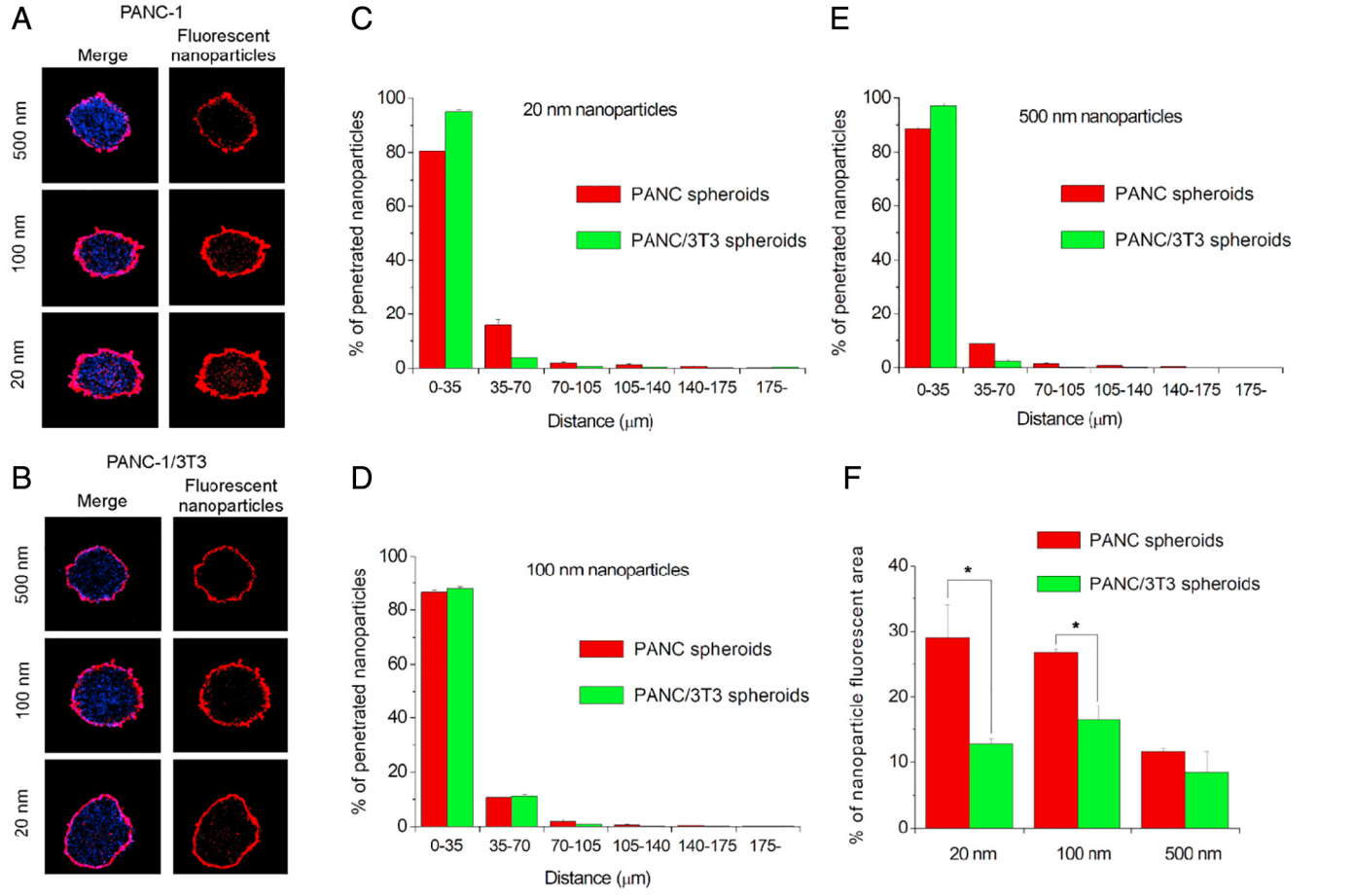

Figure 3. Analysis of nanoparticle penetration in pancreatic cancer spheroids. Distribution of 20 nm, 100 nm and 500 nm polystyrene nanoparticles (red) in PANC-1 (A) and PANC-1/NIH3T3 (B) spheroids stained with Hoechst (blue nuclei) after 24 hours of incubation. Spheroids were grown during 2 weeks with initial number of cells of 120 and 120:12 per well for PANC-1 and PANC-1/NIH3T3, respectively. All images in (A) and (B) have a size of 635 × 635 microns. (C), (D) and (E) represent quantitative analysis of 20 nm, 100 nm and 500 nm nanoparticle penetration in spheroids, respectively. (F) Quantitative analysis of a total nanoparticle uptake by homo- and heterospheroids. *$P < .05$ (Mann–Whitney U test). All values are shown as means ± SD.

simultaneously both a cause and consequence of intratumoral cross-talk between stroma, pancreatic cancer and stellate cells [28]. In particular, hypoxic conditions along with other stimuli promote activation of quiescent fibroblasts into myofibroblasts, expressing α-smooth muscle actin (α-SMA), which significantly contribute to the desmoplastic reaction [4]. Additionally, hypoxia is considered to have an impact on the metastatic potential in PDAC tumors [29]. Thus, inoculation of pre-existing hypoxic and ECM expressing microtumors rather than suspension of pancreatic cancer cells would better mimic hyperplasia of ductal epithelium at an initial stage of PDAC.

Here, we compared four types of pancreatic tumor xenografts, established by subcutaneous inoculation of 1) PANC-1 cells; 2) 10:1 mixture of PANC-1 and 3 T3 cells; 3) PANC-1 spheroids; and 4) PANC-1/3 T3 spheroids generated at the initial ratio of 10:1. It was found that only in the case of PANC-1/3 T3 spheroids all mice developed tumors, whereas for other cohorts of mice tumors developed in 80% of animals (4 of 5).

As far as the initial number of inoculated cells was different for all groups of mice, measurements of tumor size are irrelevant for direct intergroup comparison of tumor growth rates. To determine the rates of tumor growth, we fitted experimental data using Gompertz function, a mathematical model describing tumor growth [30]. Although all growth rate constants have very similar values (Supplementary Table 2), two trends were observed. First, tumors established from cells grow faster, perhaps a result of easier access of nutrients and oxygen to cancer cells, especially at early days upon inoculation, whereas cells in the spheroid core may lack in nutrients and oxygen limiting tumor expansion. Second, fibroblast-containing xenografts grow faster than counterparts established by inoculation solely of cancer cells. It should be noted that our data are in compliance with the earlier study, where co-injection of PSCs and cancer cells led to higher tumorigenicity of orthotopic xenografts [31]. Most probably, that presence of fibroblast enhances the resistance of cancer cells to serum starvation and hypoxia as reported earlier [32]. Different mechanisms may be involved in the pro-survival stimulation of cancer cells by CAFs including, for instance, IGF1 receptor-mediated [33] and β1-integrin-mediated signaling [20]. Below, we investigated β1-integrin expression and activation of this pathway in different groups of xenografts.

Characterization of ECM Production and Organization in Clinical Pancreatic Tumors, Spheroids and Cell Based Xenografts

Besides analysis of tumorigenicity of different pancreatic xenografts, another important goal was to determine such hallmarks of the tumor microenvironment as ECM production, expression of pro-

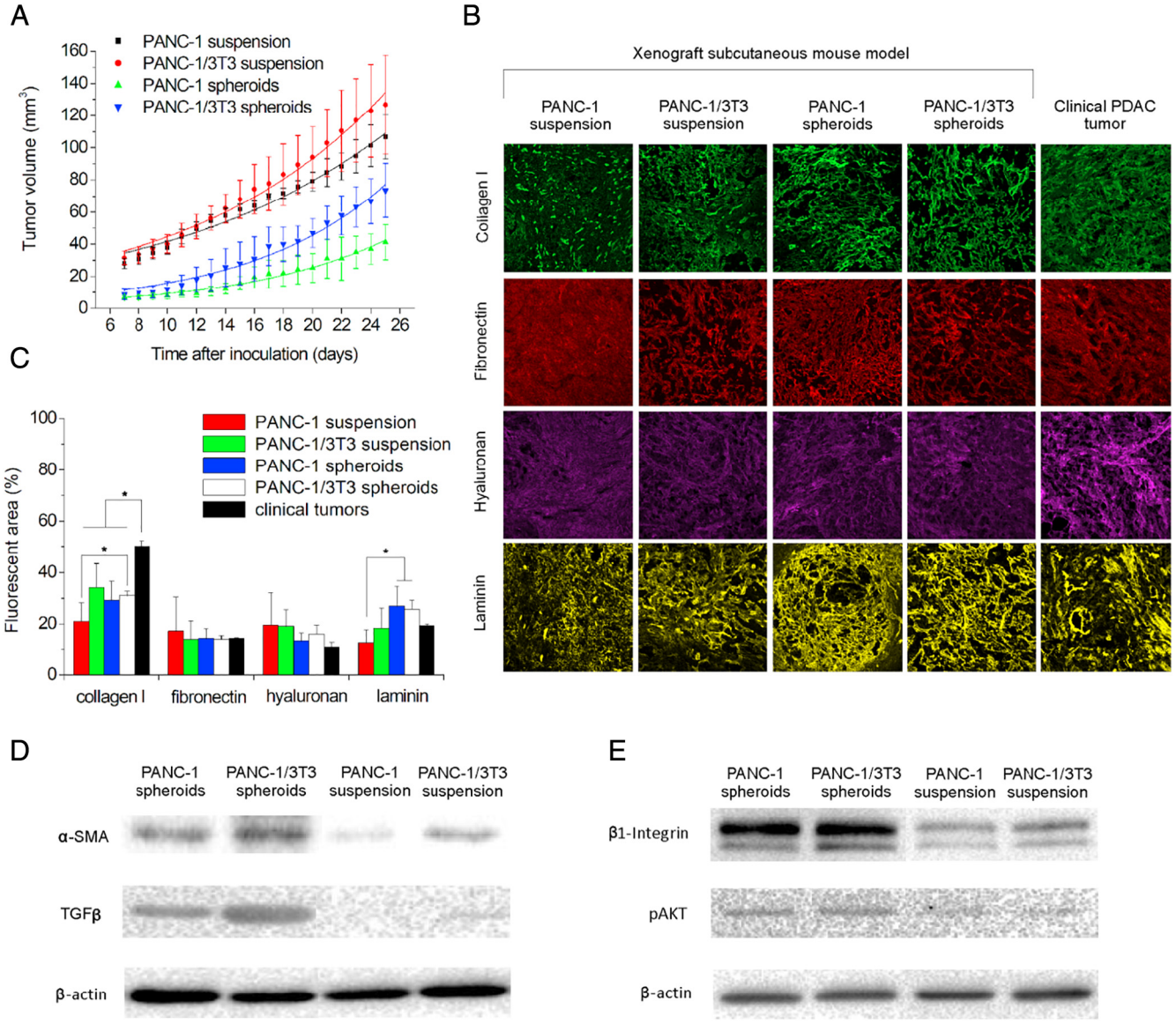

Figure 4. Characterization of different types of PANC-1 tumor xenografts. (A) Growth rates of tumor xenografts inoculated subcutaneously. Experimental data (dot scatters) were fitted with Gompertz functions (solid curves) of tumor growth. Number of animals is 4 per group. Data are shown as means ± SD. (B) Representative images of frozen tumor tissue sections stained with antibodies against different ECM components including collagen I (green), fibronectin (red), hyaluronic acid (purple), and laminin (yellow). All images have a size of 635 × 635 microns. (C) Quantitative estimation of fluorescent positive areas of ECM components in xenograft and patient PDAC tumors. Values are represented as means ± SD. Western blotting expression analysis of PDAC tumor hallmarks such as α-smooth muscle actin (α-SMA), transforming growth factor β (TGFβ), β1-integrin receptors, and activated AKT signaling pathway (pAKT) (D), (E).

fibrotic growth factors, and the level of pro-survival signaling pathway activation, as relevant to clinical tumors.

Analysis of immunofluorescent stained sections of xenograft tumor tissues and two clinical PDAC tumors resulted in some comparative observations. First, the highest level of collagen I production was detected in clinical tumors reaching almost 50% of area which is 1.5–2-fold higher than in xenografts. Interestingly, that the lowest collagen I deposition was observed in PANC-1 xenografts established by cell injection (Figure 4, *B* and *C*). It is remarkable that the character of collagen I distribution in these tumors was diffused with rare discrete bundles, whereas it was organized in a tortuous fibrillar network with thick bundles in a most of PANC-1/3 T3 cell based xenografts, in all tumors originating from spheroids, and in clinical tumors (Supplementary Fig. 2). The similar trend in architecture and organization of other ECM components such as hyaluronan, laminin and fibronectin was also observed (Supplementary Figs. 3–5). It should be noted that hyaluronan and fibronectin were deposited in a tumor tissue of xenografts in a similar extent as in clinical tumors, whereas laminin production in spheroid based tumors was even higher (Figure 4*C*). Another important observation is a very high variation of ECM production in a case of xenografts established by cell injection, whereas no significant intertumoral differences were found in the case of spheroid-based tumors.

Besides characterization of ECM production, we also characterized expression of some additional functional hallmarks of PDAC in tumor xenografts using Western blotting. It was found that

expression of transforming growth factor β (TGFβ) is significantly enhanced in tumors originating from spheroids as compared with cell based xenografts (Figure 4*D*). TGFβ is one of the key participants in PDAC cancerogenesis, which promotes EMT and tumor invasion [34]. Moreover, TGFβ activates PSCs [3,4] or subcutaneous and 3 T3 fibroblasts [35] as in the case of xenograft tumors, contributing to development of desmoplasia in clinical or model PDAC tumors, respectively. Activation of quiescent fibroblasts and the level of tumor infiltration with CAFs can be indicated by expression of α-SMA, a key marker of activated fibroblasts. We found an elevated level of α-SMA expression in spheroid tumors as compared with cell-based xenografts (Figure 4*D*) that might be a consequence of enhanced production of TGFβ in these tumors.

In terms of the observed differences in ECM architecture in spheroid and cell based tumor xenografts, we evaluated expression of β1-integrin receptors, which are involved in ECM-mediated signaling upon interaction with collagen I, fibronectin, laminin, and other components [9,11,12]. Interaction of these receptors with ECM increases metastatic potential [9,10], induces EMT [9,10], and up-regulates TGFβ1 secretion [8]. Moreover, β1-integrin receptors actively participate in assembly of fibronectin and collagen I fibrils [23,36] as mentioned above, and was confirmed in the spheroid model for fibronectin (Supplementary Fig. 1). It turned out that in xenografts originating from spheroids the level of β1-integrin receptors expression is higher than in cell-based tumors (Figure 4*E*). Usually, β1-integrin-ECM interaction activates two major signaling pathways, FAK/ROCK and PI3K/AKT [7,20,37]. PI3K/AKT pathway is frequently activated in PDAC tumors, and can be a prognostic indicator for PDAC [38]. We found a much higher amount of phosphorylated AKT (pAKT) in spheroid tumors indicating enhanced activation of this signaling pathway, as compared with cell based xenografts. This may be a result of the increased contribution of β1-integrins into induction of this pathway due to enhanced β1-integrin expression and/or altered (more fibrillar) ECM organization.

Thus, the spheroid-based xenograft model showed an altered ECM architecture with thick bundles of collagen and other components recapitulating clinical tumors along with enhanced expression of pro-survival and pro-fibrotic hallmarks.

Discussion

Desmoplastic stroma reaction is a unique characteristic of PDAC. To date, it is still unclear whether excessive ECM production constrains or promotes cancer progression [39,40]. Regardless, development of pancreatic tumor models recapitulating clinical tumors is very important for screening and testing of novel anti-cancer strategies and formulations.

In this study, we developed a 3D *in vitro* model of PDAC tumors, able to grow in size up to 2 weeks. Such a long cultivation time provides more opportunities for strong cell-to-cell interactions and formation of ECM network. Incorporation of 3 T3 fibroblasts into the spheroid model improved ECM production in microtumors. PANC-1/3 T3 heterospheroids produced a complex ECM network containing different components, including glycosaminoglycans, such as hyaluronan, and proteins such as fibrillar collagen I, fibronectin, and laminin (Figure 2). Analysis of ECM production in spheroids clarified some details of cell-ECM interplay. It was found that treatment of PANC-1/3 T3 spheroids with anti-β1-integrin IgG significantly impaired fibronectin polymerization (Supplementary Fig. 1). Additionally, lack of fibronectin production in PANC-1 homospheroids did not lead to formation of fibrillar collagen I network in contrast to heterospheroids, where fibronectin was expressed by 3 T3 fibroblasts. Both these facts elucidate an important role of fibronectin and β1-integrin receptors in ECM assembly and organization. Probably, development of novel therapeutics targeting the sites of fibronectin–fibronectin, fibronectin-collagen I, or fibronectin-β1-integrin interactions would help to reduce desmoplastic reactions in PDAC and improve efficacy of chemotherapy.

It was found that the spheroid stroma presented a significant barrier for penetration of nanoparticles. The lack of convective influx of nanoparticles into spheroid interstitium from outside in a 3D tumor model resembles the absence of the convective contribution to nanoparticle extravasation and diffusion in tumors, where interstitial fluid flux towards lymphatic capillaries is impaired due to a collapse of lymphatic drainage [25,41]. In our PANC/3 T3 spheroid model, around 90% of accumulated 100-nm particles crossed a distance less than 35 μm (Figure 3*D*). It was found earlier that intravenously injected 100-nm nanoparticles in PDAC xenograft model penetrated the tumor stroma up to 30 microns [15]. This comparison reflects the relevancy of our 3D model for estimation of nanomedicine penetration in tumor tissue.

In this study, we first translated a pancreatic cancer spheroid model *in vivo* for generation of xenograft tumors. To date, different types of animal preclinical models for human PDAC are available, and all of them have strengths and limitations. For instance, numerous transgenic mouse models reproduce human PDAC relatively closely in terms of key molecular events and morphology making them ideal for basic studies, but these models are very costly and unsuitable for analysis of therapeutic strategies and drugs [42]. Patient-derived tumor xenografts make it possible to select the best personalized chemotherapeutic regimen with predictive value over 80%, but this approach is inapplicable to most patients because it requires a long predictive patient survival and sufficient tumor tissue for establishing xenografts [27,43]. Thus, orthotopic and subcutaneous xenografts from cancer cell lines stay the most easy and commonly used animal model for rapid testing of drug efficacies, drug safety and delivery strategies. Cell based xenograft models demonstrated a moderate predictive value probably due to genetic homogeneity and lack of immune component [27]. Another weakness of these models is a limited desmoplastic reaction [42]. Some attempts to improve cell-based xenograft models were made to address these concerns. First, cancer cells can be inoculated in a mixture with PSCs to improve stroma reaction and tumorigenicity [31]. In other study, authors increased the extent of tumor fibrosis in subcutaneous murine model by co-administration of cancer cells with bFGF. It improved tumorigenicity of xenografts, increased fibrosis, and diminished extravasation and accumulation of intravenously injected 2 MDa dextran as a model macromolecule [44]. A relatively new and very promising approach to improve xenograft animal model of PDAC for translational studies is pancreatic 3D organoid based tumors. PDAC organoid is a conglomeration of cells developed from adult stem cells originating from human or mouse pancreatic tumor tissues, and embedded in a 3D matrix. Their orthotopic transplantation resulted in development of tumors recapitulating human PDAC and maintaining of phenotypic heterogeneity of the primary tumor [45–47]. Probably, further evaluation will assess the utility of this model for translational studies. The spheroid-based xenograft model developed here is highly reproducible in terms of ECM content and organization in contrast to common cell based xenografts, and recapitulated clinical PDAC tumors. Spheroid based tumors demonstrated enhanced expression of pro-fibrotic and pro-survival hallmarks as compared with tumors originating from cells. Moreover, this model holds some additional

capabilities for improvement. First, xenografts established by inoculation of 3D heterospheroids made of PSCs and cancer cells might be a more relevant model of PDAC tumors than considered here PANC-1 and PANC-1/3 T3 spheroids. Next, orthotopic transplantation is expected to be advantageous in terms of higher clinical relevancy. Furthermore, incorporation of immune cells such as regulatory T cells into the spheroid model might also impart to the model complex interplay between cancer cells, CAFs and immune system. Finally, genetic manipulations with cells forming spheroids can improve tumor-host interactions, desmoplastic reaction, tumor progression and metastatic potential, as well as detection of tumor growth in orthotopic models.

Conclusions

In this study, we developed pancreatic cancer spheroids based on cancer cell and fibroblast co-culture, and were able to produce complex multi-component ECM. These spheroids demonstrated relevant diffusion barrier function for model nanoparticles and can be exploited for rapid screening of drugs and drug delivery approaches.

Moreover, *in vivo* translation of the spheroid model significantly improved subcutaneous xenograft model of PDAC. In particular, inoculation of spheroids resulted in reproducible stroma-rich tumors with thick bundle network ECM architecture recapitulating clinical PDAC tumors. Additionally, spheroid based xenografts demonstrated higher expression of pro-fibrotic and pro-survival PDAC hallmarks as compared with cell based tumors. We believe that future development of this model will provide an effective instrument for testing of anti-cancer drugs with improved predictive value.

Acknowledgements

This project was supported by the American Cancer Society Pilot Award [11-053-01-IRG] and the South Dakota Board of Regents Competitive Research Grant Program track 1 Awards. The authors thank the patients for their invaluable contribution and consenting to the research use of their tissue.

Appendix A. Supplementary data

Supplementary data to this article can be found online at https://doi.org/10.1016/j.tranon.2018.10.003.

References

[1] Whatcott CJ, Posner RG, Von Hoff DD, and Han H (2012). Desmoplasia and chemoresistance in pancreatic cancer. In: Grippo PJ, Munshi HG, editors. Pancreat. Cancer Tumor Microenviron. Trivandrum (India): Transworld Research Network; 2012http://www.ncbi.nlm.nih.gov/books/NBK98939/, Accessed date: 4 July 2018.

[2] Tamburrino A, Piro G, Carbone C, Tortora G, and Melisi D (2013). Mechanisms of resistance to chemotherapeutic and anti-angiogenic drugs as novel targets for pancreatic cancer therapy. *Front Pharmacol* **4**, 56.

[3] Omary MB, Lugea A, Lowe AW, and Pandol SJ (2007). The pancreatic stellate cell: a star on the rise in pancreatic diseases. *J Clin Invest* **117**, 50–59. https://doi.org/10.1172/JCI30082.

[4] Zhan H-X, Zhou B, Cheng Y-G, Xu J-W, Wang L, Zhang G-Y, and Hu S-Y (2017). Crosstalk between stromal cells and cancer cells in pancreatic cancer: New insights into stromal biology. *Cancer Lett* **392**, 83–93. https://doi.org/10.1016/j.canlet.2017.01.041.

[5] Vonlaufen A, Phillips PA, Xu Z, Goldstein D, Pirola RC, Wilson JS, and Apte MV (2008). Pancreatic Stellate Cells and Pancreatic Cancer Cells: An Unholy Alliance. *Cancer Res* **68**, 7707–7710. https://doi.org/10.1158/0008-5472.CAN-08-1132.

[6] Cirri P and Chiarugi P (2011). Cancer associated fibroblasts: the dark side of the coin. *Am J Cancer Res* **1**, 482–497.

[7] Rath N and Olson MF (2016). Regulation of pancreatic cancer aggressiveness by stromal stiffening. *Nat Med* **22**, 462–463. https://doi.org/10.1038/nm.4099.

[8] Shields MA, Dangi-Garimella S, Redig AJ, and Munshi HG (2012). Biochemical role of the collagen-rich tumour microenvironment in pancreatic cancer progression. *Biochem J* **441**, 541–552. https://doi.org/10.1042/BJ20111240.

[9] Duan W, Ma J, Ma Q, Xu Q, Lei J, Han L, Li X, Wang Z, Wu Z, and Lv S, et al (2014). The Activation of β1-integrin by Type I Collagen Coupling with the Hedgehog Pathway Promotes the Epithelial-Mesenchymal Transition in Pancreatic Cancer. *Curr Cancer Drug Targets* **14**, 446–457.

[10] Shintani Y, Hollingsworth MA, Wheelock MJ, and Johnson KR (2006). Collagen I promotes metastasis in pancreatic cancer by activating c-Jun NH(2)-terminal kinase 1 and up-regulating N-cadherin expression. *Cancer Res* **66**, 11745–11753. https://doi.org/10.1158/0008-5472.CAN-06-2322.

[11] Huanwen W, Zhiyong L, Xiaohua S, Xinyu R, Kai W, and Tonghua L (2009). Intrinsic chemoresistance to gemcitabine is associated with constitutive and laminin-induced phosphorylation of FAK in pancreatic cancer cell lines. *Mol Cancer* **8**, 125. https://doi.org/10.1186/1476-4598-8-125.

[12] Topalovski M and Brekken RA (2016). Matrix control of pancreatic cancer: new insights into fibronectin signaling. *Cancer Lett* **381**, 252–258. https://doi.org/10.1016/j.canlet.2015.12.027.

[13] Sato N, Kohi S, Hirata K, and Goggins M (2016). Role of hyaluronan in pancreatic cancer biology and therapy: Once again in the spotlight. *Cancer Sci* **107**, 569–575. https://doi.org/10.1111/cas.12913.

[14] Provenzano PP and Hingorani SR (2013). Hyaluronan, fluid pressure, and stromal resistance in pancreas cancer. *Br J Cancer* **108**, 1–8. https://doi.org/10.1038/bjc.2012.569.

[15] Diop-Frimpong B, Chauhan VP, Krane S, Boucher Y, and Jain RK (2011). Losartan inhibits collagen I synthesis and improves the distribution and efficacy of nanotherapeutics in tumors. *Proc Natl Acad Sci U S A* **108**, 2909–2914. https://doi.org/10.1073/pnas.1018892108.

[16] Ware MJ, Keshishian V, Law JJ, Ho JC, Favela CA, Rees P, Smith B, Mohammad S, Hwang RF, and Rajapakshe K, et al (2016). Generation of an in vitro 3D PDAC stroma rich spheroid model. *Biomaterials* **108**, 129–142. https://doi.org/10.1016/j.biomaterials.2016.08.041.

[17] Priwitaningrum DL, Blondé J-BG, Sridhar A, van Baarlen J, Hennink WE, Storm G, Le Gac S, and Prakash J (2016). Tumor stroma-containing 3D spheroid arrays: A tool to study nanoparticle penetration. *J Control Release* **244**, 257–268. https://doi.org/10.1016/j.jconrel.2016.09.004.

[18] Hidalgo M (2010). Pancreatic cancer. *N Engl J Med* **362**, 1605–1617.

[19] Carmeliet P and Jain RK (2000). Angiogenesis in cancer and other diseases. *Nature* **407**, 249–257. https://doi.org/10.1038/35025220.

[20] Mantoni TS, Lunardi S, Al-Assar O, Masamune A, and Brunner TB (2011). Pancreatic stellate cells radioprotect pancreatic cancer cells through β1-integrin signaling. *Cancer Res* **71**, 3453–3458. https://doi.org/10.1158/0008-5472.CAN-10-1633.

[21] Attieh Y, Clark AG, Grass C, Richon S, Pocard M, Mariani P, Elkhatib N, Betz T, Gurchenkov B, and Vignjevic DM (2017). Cancer-associated fibroblasts lead tumor invasion through integrin-β3-dependent fibronectin assembly. *J Cell Biol* **216**, 3509–3520. https://doi.org/10.1083/jcb.201702033.

[22] Lee J, Yakubov B, Ivan C, Jones DR, Caperell-Grant A, Fishel M, Cardenas H, and Matei D (2016). Tissue Transglutaminase Activates Cancer-Associated Fibroblasts and Contributes to Gemcitabine Resistance in Pancreatic Cancer. *Neoplasia* **18**, 689–698. https://doi.org/10.1016/j.neo.2016.09.003.

[23] Kadler KE, Hill A, and Canty-Laird EG (2008). Collagen fibrillogenesis: fibronectin, integrins, and minor collagens as organizers and nucleators. *Curr Opin Cell Biol* **20**, 495–501. https://doi.org/10.1016/j.ceb.2008.06.008.

[24] Kleeff J, Kothari NH, Friess H, Fan H, and Korc M (2004). Adenovirus-mediated transfer of a truncated fibroblast growth factor (FGF) type I receptor blocks FGF-2 signaling in multiple pancreatic cancer cell lines. *Pancreas* **28**, 25–30.

[25] Chauhan VP, Stylianopoulos T, Boucher Y, and Jain RK (2011). Delivery of Molecular and Nanoscale Medicine to Tumors: Transport Barriers and Strategies. *Annu Rev Chem Biomol Eng* **2**, 281–298. https://doi.org/10.1146/annurev-chembioeng-061010-114300.

[26] Herreros-Villanueva M, Hijona E, Cosme A, and Bujanda L (2012). Mouse models of pancreatic cancer. *World J Gastroenterol* **18**, 1286–1294. https://doi.org/10.3748/wjg.v18.i12.1286.

[27] Hwang C-I, Boj SF, Clevers H, and Tuveson DA (2016). Preclinical models of pancreatic ductal adenocarcinoma. *J Pathol* **238**, 197–204. https://doi.org/10.1002/path.4651.

[28] Erkan M, Reiser-Erkan C, Michalski CW, Deucker S, Sauliunaite D, Streit S, Esposito I, Friess H, and Kleeff J (2009). Cancer-Stellate Cell Interactions

Perpetuate the Hypoxia-Fibrosis Cycle in Pancreatic Ductal Adenocarcinoma. *Neoplasia* **11**, 497–508. https://doi.org/10.1593/neo.81618.

[29] Lohse I, Lourenco C, Ibrahimov E, Pintilie M, Tsao M-S, and Hedley DW (2014). Assessment of Hypoxia in the Stroma of Patient-Derived Pancreatic Tumor Xenografts. *Cancer* **6**, 459–471. https://doi.org/10.3390/cancers6010459.

[30] Laird AK (1964). Dynamics of Tumour Growth. *Br J Cancer* **18**, 490–502.

[31] Hwang RF, Moore T, Arumugam T, Ramachandran V, Amos KD, Rivera A, Ji B, Evans DB, and Logsdon CD (2008). Cancer-Associated Stromal Fibroblasts Promote Pancreatic Tumor Progression. *Cancer Res* **68**, 918–926. https://doi.org/10.1158/0008-5472.CAN-07-5714.

[32] Liu Y and Du L (2015). Role of pancreatic stellate cells and periostin in pancreatic cancer progression. *Tumour Biol* **36**, 3171–3177. https://doi.org/10.1007/s13277-015-3386-2.

[33] Hirakawa T, Yashiro M, Doi Y, Kinoshita H, Morisaki T, Fukuoka T, Hasegawa T, Kimura K, Amano R, and Hirakawa K (2016). Pancreatic Fibroblasts Stimulate the Motility of Pancreatic Cancer Cells through IGF1/IGF1R Signaling under Hypoxia. *PLoS One* **11**e0159912. https://doi.org/10.1371/journal.pone.0159912.

[34] Wu Q, Tian Y, Zhang J, Zhang H, Gu F, Lu Y, Zou S, Chen Y, Sun P, and Xu M, et al (2017). Functions of pancreatic stellate cell-derived soluble factors in the microenvironment of pancreatic ductal carcinoma. *Oncotarget* **8**, 102721–102738. https://doi.org/10.18632/oncotarget.21970.

[35] Hinz B, Celetta G, Tomasek JJ, Gabbiani G, and Chaponnier C (2001). Alpha-smooth muscle actin expression upregulates fibroblast contractile activity. *Mol Biol Cell* **12**, 2730–2741.

[36] Velling T, Risteli J, Wennerberg K, Mosher DF, and Johansson S (2002). Polymerization of Type I and III Collagens Is Dependent On Fibronectin and Enhanced By Integrins α11β1and α2β1. *J Biol Chem* **277**, 37377–37381. https://doi.org/10.1074/jbc.M206286200.

[37] Falasca M, Selvaggi F, Buus R, Sulpizio S, and E. Edling C (2011). Targeting phosphoinositide 3-kinase pathways in pancreatic cancer–from molecular signalling to clinical trials. *Anticancer Agents Med Chem* **11**, 455–463.

[38] Yamamoto S, Tomita Y, Hoshida Y, Morooka T, Nagano H, Dono K, Umeshita K, Sakon M, Ishikawa O, and Ohigashi H, et al (2004). Prognostic Significance of Activated Akt Expression in Pancreatic Ductal Adenocarcinoma. *Clin Cancer Res* **10**, 2846–2850. https://doi.org/10.1158/1078-0432.CCR-02-1441.

[39] Neesse A, Algül H, Tuveson DA, and Gress TM (2015). Stromal biology and therapy in pancreatic cancer: a changing paradigm. *Gut* **64**, 1476–1484. https://doi.org/10.1136/gutjnl-2015-309304.

[40] Gore J and Korc M (2014). Pancreatic cancer stroma: friend or foe? *Cancer Cell* **25**, 711–712. https://doi.org/10.1016/j.ccr.2014.05.026.

[41] Durymanov MO, Rosenkranz AA, and Sobolev AS (2015). Current Approaches for Improving Intratumoral Accumulation and Distribution of Nanomedicines. *Theranostics* **5**, 1007–1020. https://doi.org/10.7150/thno.11742.

[42] Krempley BD and Yu KH (2017). Preclinical models of pancreatic ductal adenocarcinoma. *Chin Clin Oncol* **6**, 25. https://doi.org/10.21037/cco.2017.06.15.

[43] Cassidy JW, Caldas C, and Bruna A (2015). Maintaining Tumor Heterogeneity in Patient-Derived Tumor Xenografts. *Cancer Res* **75**, 2963–2968. https://doi.org/10.1158/0008-5472.CAN-15-0727.

[44] Sakai S, Iwata C, Tanaka HY, Cabral H, Morishita Y, Miyazono K, and Kano MR (2016). Increased fibrosis and impaired intratumoral accumulation of macromolecules in a murine model of pancreatic cancer co-administered with FGF-2. *J Control Release* **230**, 109–115. https://doi.org/10.1016/j.jconrel.2016.04.007.

[45] Huang L, Holtzinger A, Jagan I, BeGora M, Lohse I, Ngai N, Nostro C, Wang R, Muthuswamy LB, and Crawford HC, et al (2015). Ductal pancreatic cancer modeling and drug screening using human pluripotent stem cell- and patient-derived tumor organoids. *Nat Med* **21**, 1364–1371. https://doi.org/10.1038/nm.3973.

[46] Boj SF, Hwang C-I, Baker LA, Chio IIC, Engle DD, Corbo V, Jager M, Ponz-Sarvise M, Tiriac H, and Spector MS, et al (2015). Organoid models of human and mouse ductal pancreatic cancer. *Cell* **160**, 324–338. https://doi.org/10.1016/j.cell.2014.12.021.

[47] Öhlund D, Handly-Santana A, Biffi G, Elyada E, Almeida AS, Ponz-Sarvise M, Corbo V, Oni TE, Hearn SA, and Lee EJ, et al (2017). Distinct populations of inflammatory fibroblasts and myofibroblasts in pancreatic cancer. *J Exp Med* **214**, 579–596. https://doi.org/10.1084/jem.20162024.